Ozone Transfer with Optimal Design of a New Gas-Induced Reactor

Yung-Chien Hsu and Chyuan-Jih Huang
Dept. of Chemical Engineering, National Taiwan Institute of Technology, Taipei 106, Taiwan, R.O.C.

The optimal geometric design and the mass transfer of ozone for a new gas-induced reactor characterized by the installation of a draft tube and dual pitched-blade turbines were studied. Geometric factors including the impeller diameter, the length and diameter of draft tube, the liquid level, and the impeller speed were investigated to find the optimal gas utilization rate and power consumption for agitation. Furthermore, under the optimal geometric conditions, several variables including the impeller speed, the input gas flow rate, and the liquid level were investigated to reveal the volumetric mass-transfer coefficient of ozone. The optimal geometry was suggested by three empirical equations that correlated successfully the onset impeller speed for gas induction and the power consumption post gas induction with geometrical factors and operational variables. Volumetric mass-transfer coefficients of ozone were 0.8 – 1.2 min^{-1} under optimal geometric and proper operational conditions, which are comparable to the cited values in the literature.

Introduction

The agitated tank is one of the most common and important reactors that have been widely used for gas–liquid heterogeneous reactions in the chemical industry. It performs well, giving good mixing effect, better mass and heat transfers, and so forth (Joshi et al., 1982; Oldshue, 1983). However, the interaction between turbines and baffles requires high power consumption. Furthermore, recovery of the unreacted gas injected through the process liquid from the bottom of the conventional agitated tanks is rather complicated. This problem is commonly solved by linking the tanks in series or by using a compressor to recirculate the unreacted gas back to the process liquid. Both of these two methods are complex processes and may need additional accessory equipment that will increase operational costs. Agitated-tank design therefore needs to be improved for specific purposes, such as simplifying the system to obtain better gas utilization, lower power consumption, and longer gas/liquid contact time.

Hsu and Huang (1996) developed a unique protoreactor, in which, two 45° pitched-blade turbines were enclosed by a draft tube. The reactor had two major characteristics in gas induction and bubble circulation around the draft tube. Another advantage in cost saving was an improvement in utilization rate without additional accessory equipment. Since the geometry affects significantly the performance of a reactor, this work is undertaken to investigate the optimal utilization rate and power consumption.

Hsu and Chang (1995) noted previously that the most stable gas induction could be attained by fixing the space between two turbines in a narrow baffled-gas-induced reactor at one turbine diameter. Hsu and Huang (1997) also indicated that the liquid mixing time was independent of the position of the lower turbine, when it was placed above the bottom with a clearance of one-third to one-half of the tank diameter in the gas-induced reactor. The impeller diameter in a conventional gas–liquid agitated tank is generally set within a range of one-third to one-half of the tank diameter (Joshi et al., 1982; Mann, 1986). In this work, the effects of geometric factors, including the impeller diameter, the length and the diameter of draft tube, and the liquid level on the performance of the gas-induced reactor, are studied to search for an optimal geometric design. The mass transfer of the ozone/water system was also investigated. Several major operational variables that can affect the mass transfer of ozone, including impeller speed, input gas flow rate, and liquid level, are discussed.

Correspondence concerning this article should be addressed to Y.-C. Hsu.

Table 1. Experimental Geometric Parameters

Item	Range
Tank diameter (D_t)	0.17 m
Draft-tube length (L_t)	$2D_i$–$4D_i$
Draft-tube diameter (D_d)	0.47–$0.59D_t$
Impeller diameter (D_i)	0.35–$0.5D_t$
Clearance of the lower impeller and the draft tube (C)	$0.45D_t$
Impeller speed (n)	500–1,600 rpm
Working liquid level (H_d)	1.4–$2.1D_t$

Experimental Studies

The studied reactor is like the prototype previously described by Hsu and Huang (1996). The reactor is made of acrylic resin with an inner diameter (D_t) of 0.17 m. The ranges of various geometric factors under investigation are shown in Table 1. The reactor performance under different geometric designs was evaluation on the basis of the gas utilization rate and the power consumption for agitation (P, (W)).

To evaluate the gas utilization rate, a heterogeneous ozonalytic decoloration using C.I. Reactive Blue 19 dye was conducted at 25°C and pH 7. Experimental data before 90% decoloration were collected to calculate the ozone utilization rate (U_{O_3}, (%)) (Hsu and Huang, 1996). Moreover, power consumption for agitation was measured by a torque-detecting system that involves a torque meter, a monitor (Ono Sokki Co., Ltd.), an interface (Yen-Hwa Electronics), and an on-line computer. The blank and real working torque values of the shaft (T_0 and T (N·m), respectively) at an impeller speed (n, (L/s^{-1})) in each experiment were determined by the torque meter at a detection mode of 60 times per minute. The detected torque values were averaged and substituted into Eq. 1 to obtain the power consumption for agitation,

$$P = 2\pi n(T - T_0). \tag{1}$$

In addition, the mass transfer of ozone was studied at 25°C and pH 2, as adjusted by sulfuric acid. Ozone-containing gas was fed into pure water through the draft tube, and the time-dependent concentration of ozone in water was measured by a liquid-phase ozone analyzer (Seki Co.) until a steady value was reached. Calibration of the measured values was made according to the Indigo method (Bader and Hoigne, 1981). The ozone sensor was placed at the bottom of the vessel where the bubbles were being kept from hitting the tip of the sensor. Because of the extremely low solubility of ozone, the resistance arising from gas-film diffusion can be neglected with respect to that of liquid-film diffusion, thus limiting the mass transfer rate of ozone from the gas into liquid phase only by liquid-film diffusion (Sotelo et al., 1989; Gould and Ulirsch, 1992; Munter et al., 1993). At 25°C, pH 2, and mixing times of not more than 15 seconds by fast agitation (Hsu and Huang, 1996), and assuming thorough mixing, the effect of the self-decomposition of ozone on its mass transfer can be neglected (Sotelo et al., 1987). Hence, ozone mass balance in the liquid phase can be expressed by Eq. 2 (Roth and Sullivan, 1981). Upon integration, Eq. 2 yields Eq. 3,

$$\frac{dC_L}{dt} = k_L a(C^* - C_L) \tag{2}$$

$$\ln\left(\frac{C^*}{C^* - C_L}\right) = k_L a \cdot t, \tag{3}$$

where C_L and C^* are the ozone concentration and the ozone equilibrium concentration (g/m^3), respectively, in the liquid phase. By substituting the time-dependent concentration of ozone (C_L) into Eq. 3, the volumetric mass-transfer coefficient of ozone [$k_L a$ (min^{-1})] can be obtained from the initial slope in a plot of $\ln[C^*/(C^* - C_L)]$ vs. the contact time [t (min)].

Results and Discussion

Optimal geometric design for the gas-induced reactor

Several geometric factors are considered as follows.

Length of the Draft Tube. In the gas-induced reactor, the lower turbine was placed at the same level as the bottom of the draft tube, while the space between the two turbines was fixed at a distance of one turbine diameter. If the draft tubes are too short, the flow-controlling effect will be weakened. In contrast, for draft tubes that are too long, the effective downward pumping force of the turbines will be diminished to a greater extent, because of the interference between the turbines and the inner baffles. Consequently, the lengths of the draft tube [L_t (m)] were selected at two to four times the impeller diameter [D_i (m)]. The results in Table 2 illustrate the effects of impeller speed on the ozone utilization rate and specific power consumption [P/V (kW/m^3)] by different draft-tube lengths. An increase in the impeller speed was found to increase the specific power consumption as well as the ozone utilization rate. The highest ozone utilization rate, also with the lowest power consumption, was obtained with the draft-tube length set at twice the impeller diameter. A

Table 2. Effects of Draft-Tube Length on the Ozone Utilization Rate and the Specific Power Consumption at Constant Dosing Rate of Ozone

L_t/D_i	n (min^{-1})	U_{O_3} (%)	P/V (kW/m^3)
2.0	1,100	95.63	0.104
2.0	1,200	96.25	0.121
2.0	1,300	97.65	0.142
2.0	1,400	98.12	0.168
2.5	1,100	84.64	0.114
2.5	1,200	90.98	0.140
2.5	1,300	94.98	0.166
2.5	1,400	98.12	0.186
3.0	1,100	93.59	0.114
3.0	1,200	95.29	0.145
3.0	1,300	96.09	0.169
3.0	1.400	97.40	0.191
3.5	1,100	93.60	0.105
3.5	1,200	95.05	0.127
3.5	1,300	97.24	0.149
3.5	1,400	98.32	0.169

Note: 25°C, pH = 7 ± 0.2, D_i = 0.06 m, D_t = 0.17 m; ozone input: concentration = 20 g/Nm^3; flow rate = 303.5 NL/h; liquid volume = 7 L; utilization rate calculated: data based on 90% decoloration.

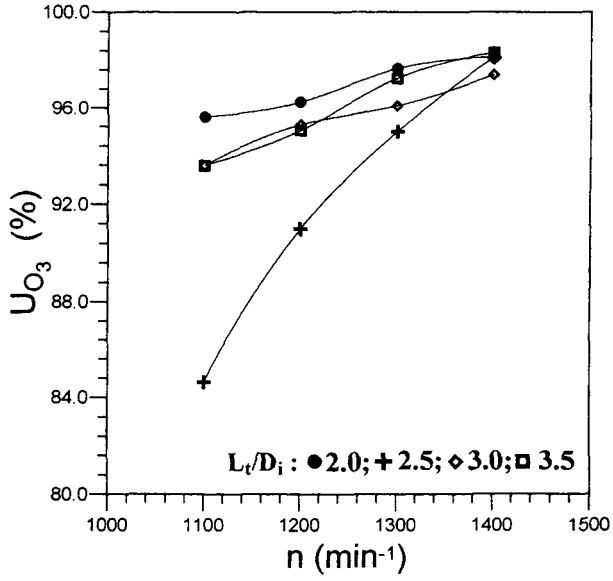

Figure 1. Ozone utilization rate vs. impeller speed under different draft-tube lengths.

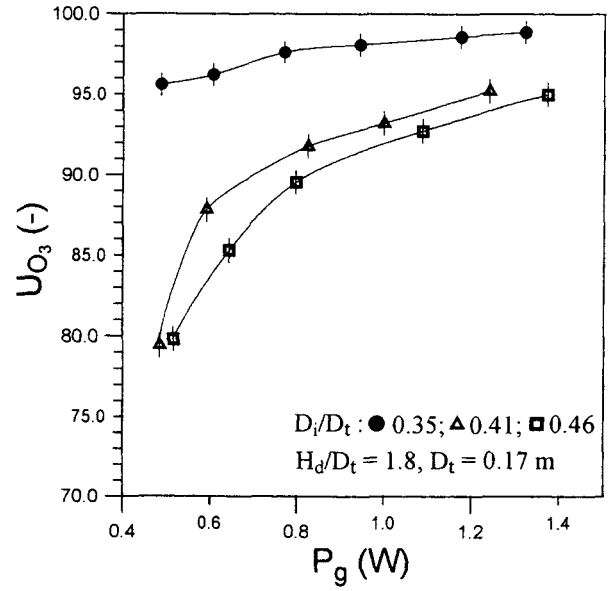

Figure 2. Ozone utilization rate vs. gassed power consumption under different impeller diameters.

95% ozone utilization rate was obtained at the lowest impeller speed (1,100 rpm) (Figure 1). Also, from the flow pattern, the draft tube with length $L_t = 2D_i$ was seen to provide the most stable gas induction and smoothest bubble circulation around the draft tube. This phenomenon was not found with longer draft tubes. The interference and the constraint on turbines from a draft tube with inner baffles were found to increase, causing the reduction of the pumping capacity. More fresh gas in the draft tube rose through the draft tube and escaped to the gas phase above the liquid, while bubbles in the annulus area between the tank body and the draft tube had more difficulty flowing into the draft tube. The gas utilization rate consequently decreased. Thus, $L_t = 2D_i$ was considered to be the optimal length for the draft tube.

Diameters of the Impeller and the Draft Tube. By referring to conventional-agitated tanks (Joshi et al., 1982; Mann, 1986), the range of the impeller diameters to be studied was selected to be from $D_t/3$ to $D_t/2$ for effective bubble chopping and dispersion. Also, the inner diameter of the draft tube was set at just slightly larger than the impeller diameter in order to reinforce the downward pumping force, while the baffle width in the draft tube was fixed at one-twentieth the inner diameter of the draft tube (Hsu and Chang, 1995). It was found that with an increase in the impeller diameter the onset impeller speed required for gas induction [n_c (min^{-1})] was significantly decreased, for example, the onset speed decreased from 1,010 rpm to 720 rpm with a corresponding increase in impeller diameter from $0.35D_t$ to $0.46D_t$. However, power consumption increases as the impeller diameter increases. The relationship between the impeller diameter and the ozone utilization rate at different power inputs (alternatively, the impeller speeds) is shown in Figure 2. As shown in Figure 2, the impeller with a diameter of $0.35D_t$ attains the highest ozone utilization rate (above 95%) at the least power consumption for agitation, which was optimal. Although other impellers with a diameter of $0.41D_t$ or $0.46D_t$ showed gas induction at much lower speeds, the ozone utilization rates obtained were significantly much less. Consequently, in this work, the impeller diameter was fixed at $D_i = 0.35D_t$, while the corresponding inner diameter of draft tube was set at $D_i = 0.47D_t$.

Clearance for Lower Turbine with Draft Tube. In general, the impeller clearance [C (m)] has always been fixed in the range of $D_t/4$ to $D_t/2$, where D_t is the tank diameter while the clearance for the lower turbine used in this study was fixed at $C = 0.45D_t$. With a clearance of shorter than $D_t/3$, the pumped flow from the draft tube would bump the tank bottom, thus consuming more power. However, with a clearance of larger than $D_t/2$, a dead zone was easily formed above the tank bottom. In addition, Hsu and Huang (1997) investigated the mixing times of a similar gas-induced reactors and concluded that the clearance in the range of $D_t/3$ to $D_t/2$ did not show significantly different effects on the mixing times post gas induction. Thus, the clearance for the lower turbine as well as the draft tube, $C = 0.45D_t$, was found to be the most feasible.

Liquid Levels. In conventionally baffled agitated tanks, the operational liquid level was normally set as high as one tank diameter for good gas/liquid contact and dispersion (Mann, 1986). However, it was found that the present reactor could obtain gas induction as the working operational liquid level [H_d (m)] was increased to twice the tank diameter, because it did not use baffles on the tank wall and because the flow was controlled by the draft tube. Results indicate that the onset speed increased as the operational liquid level increased, which may need more power consumption. The specific power consumption nevertheless remained almost unchanged. Also, the ozone utilization rates were found to exceed 95% (data not shown here) under the investigated conditions. Similar results had previously been reported in a prototype reactor (Hsu and Huang, 1996). This gas-induced reactor is feasible for different working liquid levels. Liquid levels of 1.8 to 2 times the tank diameter are recommended as the best working levels because of the increased treatability of a reactor.

Table 3. Design Characteristics Adopted for the Setup of the Present Gas-Induced Reactor

Item	Geometric Design	Reference
Kind of impeller	45° pitched-blade turbine	Chapman et al. (1983), Warmoeskerken and Smith (1984), Mann (1986); Bujalski and Nienow (1990)
Number of impellers	2	Oldshue (1983), Hsu and Chang (1995)
Number of impeller blades	6	Oldshue (1983), Chapman (1983)
Diameter of impeller	$0.35D_t$	This work
Width of blade	$D_i/8$	This work
Distance between two impellers	D_i	Hsu and Chang (1995)
Clearance of lower impeller	$0.45D_t$	Hsu and Huang (1997)
Clearance of draft tube	$0.45D_t$	Hsu and Huang (1997)
Draft-tube length	$2D_i$	This work
Draft-tube diameter	$0.47D_t$	This work
Working liquid level	$1.4D_t$–$2.0D_t$	This work
Recommended liquid level	$1.8D_t$–$2.0D_t$	This work

Note: $D_t = 0.17$ m.

The optimal geometric design of this gas-induced reactor, together with the cited ones, is shown in Table 3.

Onset speed for gas induction and power consumption post gas induction

Gas induction is considered to be a major characteristic function of the gas-induced reactor. The impeller speed has to be maintained beyond the onset point, that is, n_c (min^{-1}), in order to assure a stable gas induction and a steady recycling flow pattern as well. The onset speeds for gas induction under different geometric conditions and the power consumption post gas induction are discussed next.

Onset Speed for Gas Induction. The onset speed for the gas induction is defined as the impeller speed at which the gas above the liquid surface could be critically sucked into the liquid through the draft tube in ungassed conditions. At higher speeds, the gas in the central gas vortex can be chopped and distributed by the turbines and the draft tube. Determination of this impeller speed was carried out in this work by using the relationship between the impeller speed and the power consumption, as shown in Figure 3 as well as the visual observation of the flow phenomena. In Figure 3, the break points indicate the onset points for gas induction, which are considered a result of the change of physical property due to gas entrained into the liquid phase by turbines. From experimental studies, it was found that gas induction depended significantly not only on the impeller speed but also on the impeller diameter and working liquid level [H_d (m)]. Larger impellers provide greater pumping force. The onset thus occurs at lower impeller speeds. A higher working liquid level brings a greater submerged depth of the turbines [$(H_d - H_i)$ (m), where H_i expresses the clearance of the upper turbine] and, consequently, a higher onset speed is required. Sawant and Joshi (1979) as well as Tanaka and Izumi (1987) have also cited the importance of the submerged turbine depth for gas induction. By dimensional analysis and data regression, Eq. 4 is deduced to correlate the onset speed for gas induction with the relevant geometric factors:

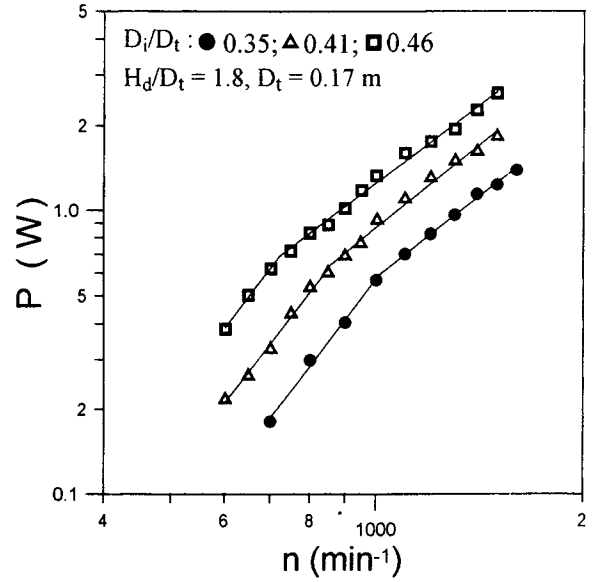

Figure 3. Ungassed power consumption vs. impeller speeds.

$$N_{Fr,c} = 0.35[(H_d - H_i)/D_t]^{0.97}(D_i/D_t)^{-1.46}, \qquad (4)$$

where $N_{Fr,c}$ is the Froude number at onset speed. A comparison between the observed and the calculated (by Eq. 4) $N_{Fr,c}$ is shown in Figure 4. The maximum deviation is estimated to be ±6%, implying that Eq. 4 is adequate for predicting the onset speed for gas induction.

The Power-Consumption Post Gas Induction. Under ungassed conditions, the power-consumption post gas induction of the gas-induced reactor can be described by Eq. 5:

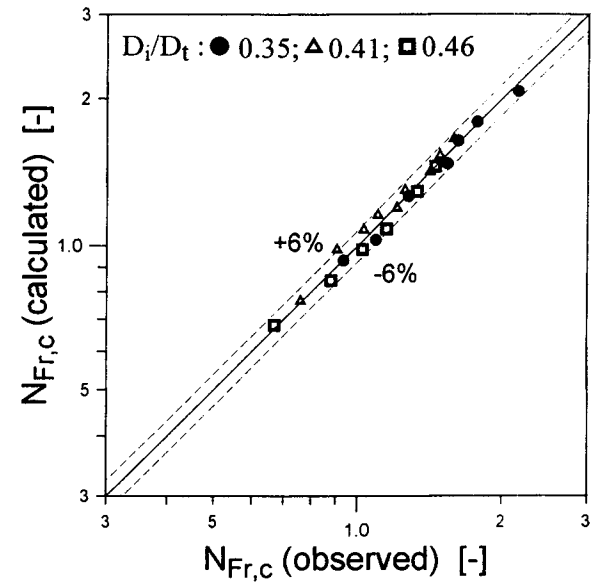

Figure 4. Observed vs. calculated Froude number obtained by Eq. 4.

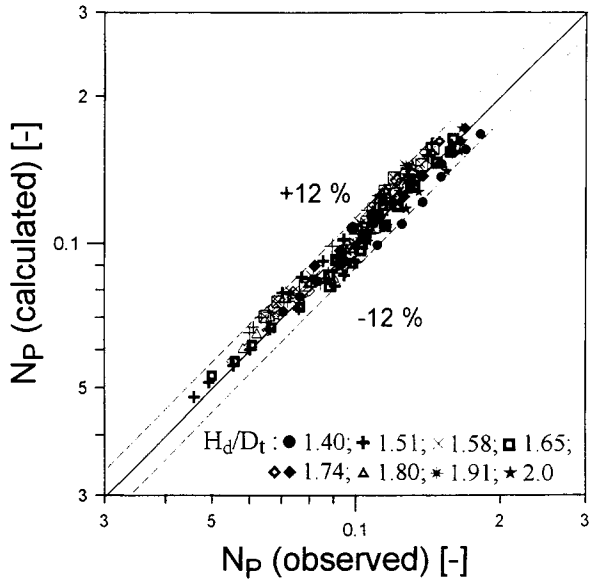

Figure 5. Observed vs. calculated ungassed power number obtained by Eq. 5.

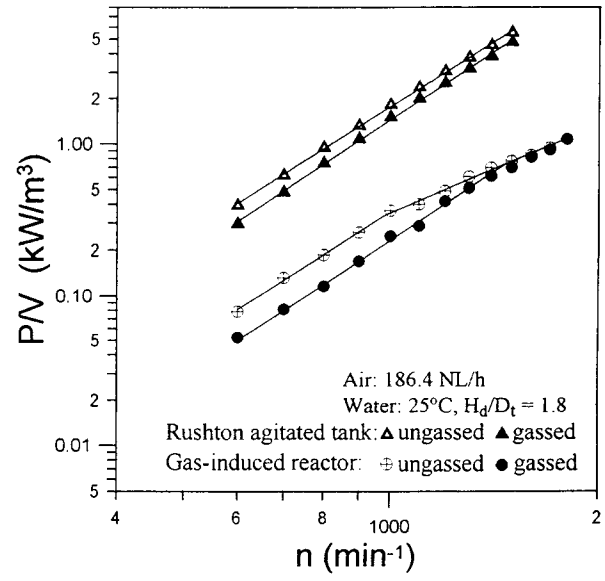

Figure 6. Power consumption for agitation: gas-induced reactor vs. Rushton agitated tank.

$$N_P = 4.46\times10^{-2}\, N_{Fr}^{-0.57}[(H_d - H_i)/D_t]^{0.53}(D_i/D_t)^{-1.43}, \quad (5)$$

where N_p is the power number under the ungassed condition. A comparison between the observed and the calculated (by Eq. 5) N_p is shown in Figure 5. The maximum deviation was found to be $\pm 12\%$. This empirical equation is useful for predicting the power-consumption post gas induction under ungassed conditions. Furthermore, as indicated in Eq. 5, the exponent of the Froude number was found to be -0.57, that is, it ranged between the exponent of an unbaffled agitated tank (-1) and a narrow-baffled agitated tank (-0.31) (Hsu and Chang, 1995), implying that a central gas vortex can more easily entrain the gas into the liquid. Equation 5 also expresses the dependence of the liquid level and the impeller diameter on the power number.

As the gas-induced reactor was applied to a gas–liquid reaction, the just-cited optimal geometric parameters, as well as gassing in the draft tube, were adopted to obtain a high gas utilization rate and low power consumption for agitation. The power consumption will therefore vary, depending on the ungassed or gassed conditions. Equation 6 is an empirical equation correlating the gassed power-consumption post gas induction with the experimental variables under a proper low gassed flow rate (303.5 NL/h), as suggested by Hsu and Huang (1996),

$$N_{pg} = 9.5\times10^{-2}\, N_{Fr}^{-0.058}[(H_d - H_i)/D_t]^{0.234}, \quad (6)$$

where N_{pg} denotes the power number under gassed conditions. The maximum deviation of Eq. 6 was, from experimental results, estimated to be $\pm 12\%$. In contrast to Eq. 5, Eq. 6 presents lower power consumption when gassing in the draft tube in the gas-induced reactor. Similar empirical equations were obtained for different impellers. Because they are not optimal, the results are not shown here.

Moreover, when compared with the Rushton agitated tank, as shown in Figure 6, under the conditions of either gassed or ungassed, the gas-induced reactor always showed lower power consumption at the same impeller speeds. Power consumption for the gas-induced reactor operated at high impeller speeds (e.g., 1,100 rpm), approximately equal to that of the Rushton agitated tank operated at 600 rpm, that is, although the gas-induced reactor requires a high impeller speed to initiate gas induction, it still requires less power.

Parameters affecting the mass transfer of ozone

Effect of the Impeller Speed. Experimental results of the volumetric mass-transfer coefficient of ozone are listed in Table 4. The coefficient was found to increase as the impeller speed increased, and then became steady at high impeller speeds. At the proper low input flow rate of 303.5 NL/h, an unstable central gas vortex was created at the center of the liquid surface, spinning at a speed up to 800 rpm. The trailing vortex occurred more easily at the tips of the impeller blade during the gassed conditions (Smith, 1985). When a large amount of fresh ozone was introduced, it would rise by converging to break up the motion of the central vor-

Table 4. Mass-Transfer Coefficients of Ozone Obtained Under Different Operational Conditions

Impeller Speed (min^{-1})	Gas Flow Rate (NL/h)	H_d/D_t	k_La (min^{-1})
800	303.5	1.82	0.436
950	303.5	1.82	0.693
1,100	303.5	1.82	0.818
1,250	303.5	1.82	1.024
1,400	303.5	1.82	1.073
1,100	186.4	1.82	0.605
1,100	420.5	1.82	1.04
1,100	537.6	1.82	1.036
1,100	303.5	1.51	1.166
1,100	303.5	1.65	1.063
1,100	303.5	1.74	0.958
1,100	303.5	2.00	0.693

Note: 25°C, pH 2, input ozone concentration = 20 g/Nm^3; D_t = 0.17 m.

tex, so only a few bubbles could be retained in the liquid. A poor mass transfer rate resulted. As the impeller speed was increased to 1,100 or 1,250 rpm, stable gas induction was formed without a concentration of gas bubbles. A larger amount of fresh gas was therefore broken and distributed by the two turbines, and was thus easily recirculated around the draft tube. Gas holdup in liquid increased from 0.5 to 2.4%. Bubbles with a diameter of 2.5–3 mm, as determined photographically, were reported to possess a better gas/liquid mass transfer (Calderbank, 1959). Moreover, by film theory, liquid film can be thinned down by increasing the agitation speed, thus increasing the mass transfer rate. However, over 1,400 rpm, no further significant increase in the mass-transfer coefficient was observed, a maximum value having thus been reached. Similar results were reported by Sotelo et al. (1989) for a conventional agitated tank.

Effect of the Input Gas Flow Rate. As shown in Table 4, an increase in the input gas flow rate can increase the volumetric mass-transfer coefficient of ozone in the gas-induced reactor. However, the effect was not obvious at high input gas flow rates due to inefficient gas induction. At lower input gas flow rates and proper high impeller speed (1,100 rpm), a stable central gas vortex was formed. The fresh/recycled mixed gas could thus be chopped and dispersed by two turbines. The gas holdup, for example, increased from 2.4 to 3.5% as the flow rates increased from 303.5 to 420.5 NL/h, and hence the volumetric mass-transfer coefficient of ozone was also increased. At too high input gas flow rates in the draft tube, the trailing vortices easily occur at lower impeller speeds. As a consequence, gas induction was weakened with more fresh gas flowing upward through the draft tube. Moreover, Nishikawa et al. (1981) stated that mass transfer tended to become agitation-controlled when the impeller speed increased, and that the dependence of input gas flow rate on the mass-transfer coefficient will be reasonably decreased. As a result, in the gas-induced reactor, better mass transfer was achieved at lower gas flow rates with highly concentrated input.

Effect of Working Liquid Level. As shown in Table 4, a lower liquid level can provide a higher volumetric mass-transfer coefficient of ozone. Larger gas holdup, as well as better turbulence, were produced at the lower working liquid levels. Owing to the forced recirculation of bubbles by the turbines, most of the bubbles tend to distribute around the draft tube. The gas holdup with the turbulence may increase with the decrease in the working liquid level. For instance, the gas holdup increased from 2.4 to 3.4% as the H_d/D_t ratio decreased from 1.82 to 1.65. The capability for gas induction may also be enhanced by a reduction in the submerged depth of the two turbines. The volumetric mass-transfer coefficient of ozone can thus increase when the working liquid level at a constant proper input gas flow rate and impeller speed decreases. However, in view of the gas utilization rate and specific power consumption, a satisfactory gas utilization rate can be attributed to a longer circulation pathway or gas/liquid contact time. The specific power consumption for agitation does not greatly increase with the increase in the working liquid level under stable gas induction (Hsu and Hang, 1996). Overall, in spite of a lower mass transfer rate, a higher working liquid level still has the characteristics of a high gas utilization rate and less power consumption for agitation.

The volumetric mass-transfer coefficient of ozone obtained under the recommended geometric and proper operational conditions were 0.8–1.2 min^{-1}, which was comparable to the values of 1.08, 1.14 and 0.98 min^{-1} that were obtained, respectively, by Prengle et al. (1975), Sheffer and Esterson (1982) and Hawash et al. (1990) in an organics-free system. However, the values are slightly smaller than the 1.24 min^{-1} reported by Farooq and Ahmed (1989) for ozone in an aqueous system involving a low-level chemical reaction.

Conclusion

This study presents an optimal geometric design for a new gas-induced reactor. The recommended optimal geometric factors, including $D_i = 0.35D_t$, $D_d = 0.47D_t$, $L_t = 2D_i$, $H_d = 1.8–2.0D_t$, were obtained on the basis of the gas utilization rate and the power consumption for agitation. The volumetric mass-transfer coefficients of ozone obtained under recommended geometric and proper operational conditions were 0.8–1.2 min^{-1}, which are comparable to those obtained in conventional agitated tanks. Both the impeller speed and the input gas flow rate, if properly low, have a positive effect on the mass transfer of ozone. Higher working liquid levels give rise to smaller volumetric mass-transfer coefficients of ozone. However, high working liquid levels, such as $1.8–2.0D_t$, can still provide a good performance for required specific purposes. Three correlation equations were used to predict the onset speed for gas induction and the power-consumption post gas induction. Compared with the Rushton agitated tank, the gas-induced reactor requires less power, although it requires a high impeller speed to initiate gas induction.

Acknowledgment

The authors thank the National Science Council of the Republic of China for its financial support under grant NSC85-2211-E-011-027.

Literature Cited

Bader, H., and J. Hoigne, "Determination of Ozone in Water by the Indigo Method," *Water Res.*, **15**, 449 (1981).

Bujalski, W., and A. W. Nienow, "The Use of Upward Pumping 45° Pitched Blade Turbine Impeller in Three-Phase Reactors," *Chem. Eng. Sci.*, **45**(2), 415 (1990).

Calderbank, P. H., "Physical Rate Processes in Industrial Fermentation. Part II: Mixing Transfer Coefficient in Gas-Liquid Contacting with and Without Mechanical Agitation," *Instn. Chem. Engr.*, **37**, 173 (1959).

Chapman, C. M., A. W. Nienow, M. Cooke, and J. C. Middleton, "Particle-Gas-Liquid Mixing in Stirred Vessels. II: Gas-Liquid Mixing," *Chem. Eng. Res. Des.*, **61**, 82 (1983).

Farooq, S., and M. Ahmed, "Modeling of an Ozone-Wastewater System's Kinetics," *Water Res.*, **23**, 809 (1989).

Gould, J. P., and G. V. Ulirsch, "Kinetics of the Heterogeneous Ozonation of Nitrated Phenols," *Water Sci. Technol.*, **26**(1–2), 169 (1992).

Hawash, S., N. El-Ibiari, and G. El-Diwani, "Study of Ozonation Reaction of Phenolic Effluents," *Waste Manage.*, **10**, 269 (1990).

Hsu, Y.-C., and H.-C. Chang, "Onset of Gas Self-Induction and Power Consumption after Gas Induction in an Agitated Tank," *J. Chem. Tech. Biotechnol.*, **64**, 137 (1995).

Hsu, Y.-C., and C.-J. Huang, "Characteristics of a New Gas-Induced Reactor," *AIChE J.*, **42**(11), 3146 (1996).

Hsu, Y.-C., and K.-F. Huang, "Effects of Geometrical Factors on Liquid Mixing in a Gas-Induced Agitated Tank," *J. Chem. Technol. Biotech.*, **68**, 222 (1997)

Joshi, J. B., A. B. Pandit, and M. M. Sharma, "Mechanically Agitated Gas-Liquid Reactors," *Chem. Eng. Sci.*, **37**, 813 (1982).
Mann, R., "Gas-Liquid Stirred Vessel Mixers: Towards a Unified Theory Based on Networks-Of-Zones," *Chem. Eng. Res. Des.*, **64**, 23 (1986).
Munter, R., S. Preis, S. Kamenev, and E. Siirde, "Methodology of Ozone Introduction into Water and Wastewater Treatment," *Ozone Sci. Eng.*, **15**, 149 (1993).
Nishikawa, N., M. Nakamura, H. Yagi, and K. Hashimoto, "Gas Absorption in Aerated Mixing Vessels," *J. Chem. Eng. Jpn.*, **14**, 219 (1981).
Oldshue, J. Y., *Fluid Mixing Technology*, McGraw-Hill, New York (1983).
Prengle, J. R. H. W., C. G. Hewes, and C. E. Mank, "Oxidation of Refractory Materials by Ozone with Ultraviolet Radiation," *Proc. Int. Symp. Ozone Technology*, p. 224 (1975).
Roth, J. A., and D. E. Sullivan, "Solubility of Ozone in Water," *Ind. Eng. Chem. Fundam.*, **20**, 137 (1981).
Sawant, S. B., and J. B. Joshi, "Onset Impeller Speed for Onset of Gas Induction in Gas-inducing Types of Agitated Contacts," *Chem. Eng. J.*, **55**, 338 (1979).
Sheffer, S., and G. L. Esterson, "Mass Transfer and Reaction Kinetics in the Ozone/Tap Water System," *Water Res.*, **16**, 383 (1982).
Smith, J. M., *Dispersion of Gases in Liquid: The Hydrodynamics of Gas Dispersion in Low Viscosity Liquids, Mixing of Liquid by Mechanical Agitation*, Gordon & Breach, New York, p. 139 (1985).
Sotelo, J. L., F. J. Beltran, F. J. Benitez, and J. Beltran-Heredia, "Henry's Law Constant for the Ozone-Water System," *Water Res.*, **23**(10), 1239 (1989).
Sotelo, J. L., F. J. Benitez, and J. Beltran-Heredia, "Ozone Decomposition in Water: Kinetics Study," *Ind. Eng. Chem. Res.*, **26**, 39 (1987).
Tanaka, M., and T. Izumi, "Gas Entrainment in Stirred-Tank Reactors," *Chem. Eng. Res. Des.*, **65**, 195 (1987).
Warmoeskerken, M. M. C. G., and J. M. Smith, "Gas-Liquid Dispersion with Pitched Blade Turbine," *Chem. Eng. Commun.*, **25**, 11 (1984).

Manuscript received Jan. 13, 1997, and revision received Apr. 24, 1997.